



ELSEVIER

Available online at www.sciencedirect.com

SCIENCE @ DIRECT®

Intermetallics 12 (2004) 1089–1096

Intermetallics

www.elsevier.com/locate/intermet

Effect of Zr-content on the oxidation and phase transformation of Zr-base amorphous alloys in air

H.H. Hsieh^{a,*}, W. Kai^a, R.T. Huang^b, M.X. Pan^c, T.G. Nieh^d

^a*Institute of Materials Engineering, National Taiwan Ocean University, Keelung 20224, Taiwan, ROC*

^b*Department of Engineering and System Science, National Tsing-Hua University, HsinChu 30013, Taiwan, ROC*

^c*Institute of Physics, Chinese Academy of Science, Beijing 100080, China*

^d*Department of Materials Science and Engineering, The University of Tennessee, Knoxville, TN 37996–2200, USA*

Abstract

The oxidation and phase transformation of three Zr-base amorphous alloys, Zr–20Cu–12Ni–10Al–5Ti (Zr53), Zr–30Cu–10Al–5Ni (Zr55), and Zr–15Cu–10Al–10Ni (Zr65), were studied over the temperature range of 300–500 °C in dry air. Oxidation kinetics of these alloys generally followed a parabolic rate law at $T > 350$ °C, but linear kinetics was obeyed at 300–350 °C. It was found that Zr65 was the most oxidation-resistant alloy among the three alloys studied. Scales formed on the alloys during oxidation consisted of mainly tetragonal- and monoclinic-ZrO₂ (t- and m-ZrO₂), and minor CuO and NiO (only detected in Zr53). The amount of m-ZrO₂ formed strongly depends upon the alloy composition, exposure time, and temperature. TEM results showed that a significant amount of nano-grained Zr₂Cu polycrystals formed beneath the amorphous oxide-scale in Zr53, indicating phase transformation has taken place. By contrast, Zr55 and Zr65 amorphous substrates transformed into Zr₂Cu and ZrAl after oxidation.

© 2004 Elsevier Ltd. All rights reserved.

Keywords: B. Oxidation; B. Phase transformation; B. Glasses, metallic

1. Introduction

Zr-base BMGs have the best glass forming ability and are considered as precursor materials for use of their static and dynamic mechanical properties in many structures [1–3]. During the past decade, many researchers studied the mechanical properties and crystallization behavior of BMGs. However, limited work has been devoted to the study of oxidation of BMGs. To use BMG for high-temperature structures in an oxidizing environment, an understanding of the oxidation behavior is needed.

Several investigations of oxidation behavior of Zr-base bulk amorphous alloys are available in the literatures [4–7]. It was reported that oxidation kinetics of the alloys in air at various temperatures follows a parabolic law. The oxide scale formed consists mainly of a mixture of t- and m-ZrO₂, although small amounts of the oxides of other alloying elements were also detected.

The annealing of metallic glasses above their glass transition temperatures leads to the formation of nanocrystals [8–10]. Recently, oxidation resistance was also found to significantly improve when amorphous BMG was

transformed into nanocrystalline microstructure [9]. An increase in strength has been observed in a number of nanocrystalline-amorphous alloys formed by annealing [10]. In this paper, we present the oxidation behavior of three Zr-base BMGs, the formation of tetragonal-to-monoclinic ZrO₂ with respect to exposure time, and the formation of other oxides and phase transformation after oxidation.

2. Experimental

Bulk metallic glasses (Zr53, Zr55, Zr65, in at.%) were fabricated by dropping the melt in a water-cooled copper mold [11]. These BMG alloys were initially sliced into 2.5 × 2 × 1.5 mm³ rectangle-shape samples (~60 mg in weight) using a low-speed diamond saw, ground and polished down to 0.05-μm diamond paste, cleaned with acetone, and dried before oxidation tests. To characterize the glass transition temperature, T_g , of the three BMGs, thermal properties were measured in argon using differential scanning calorimetry (DSC, Dupont 2000) at a heating rate of 0.167 K/s.

Oxidation experiments were carried out in dry air using a thermogravimetry analyzer (TGA, SETARAM Model

* Corresponding author.

TG92). The net flow-rate of high-pure air (>99.99%) was kept constant at 40 cm³/min throughout each test.

3. Results and discussion

3.1. DSC measurement

DSC curves of the three BMGs measured at a heating rate of 0.167 k/s from 200 to 700 °C are shown in Fig. 1.

These alloys reveal sequential phase transition from amorphous state to the glass transition region, supercooled liquid region, crystallization reaction region, and fully crystallized state. Zr53 and Zr65 are noted to have two distinct exothermic peaks during crystallization, while Zr55 exhibits only one peak during crystallization. The estimated T_g and crystallization temperature, T_x , for the three BMGs are listed in a table following the DSC curves. It is evident that Zr55 shows the largest supercooled liquid region ($\Delta T = T_x - T_g$) among

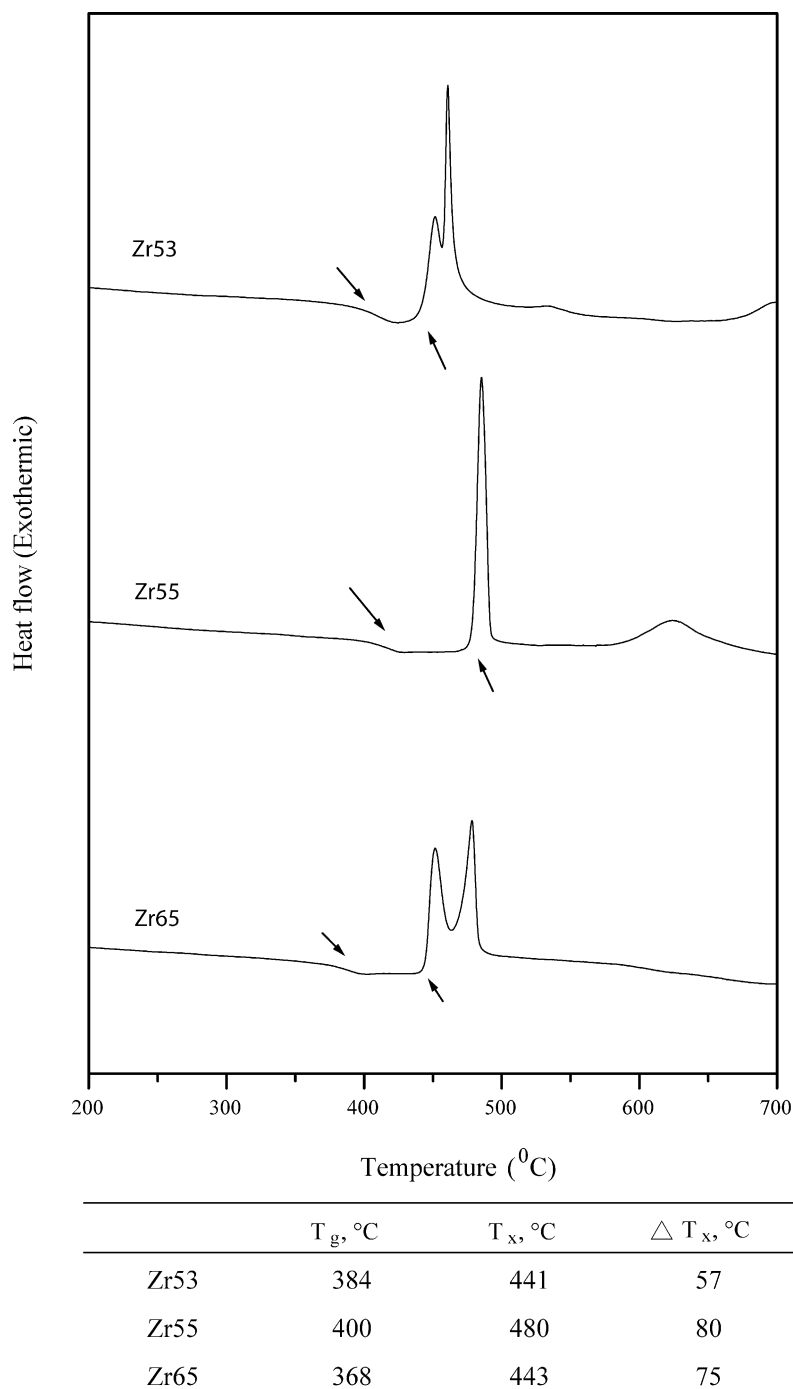


Fig. 1. DSC curves of three Zr-base metallic glasses obtained at a heating rate of 0.167 k/s.

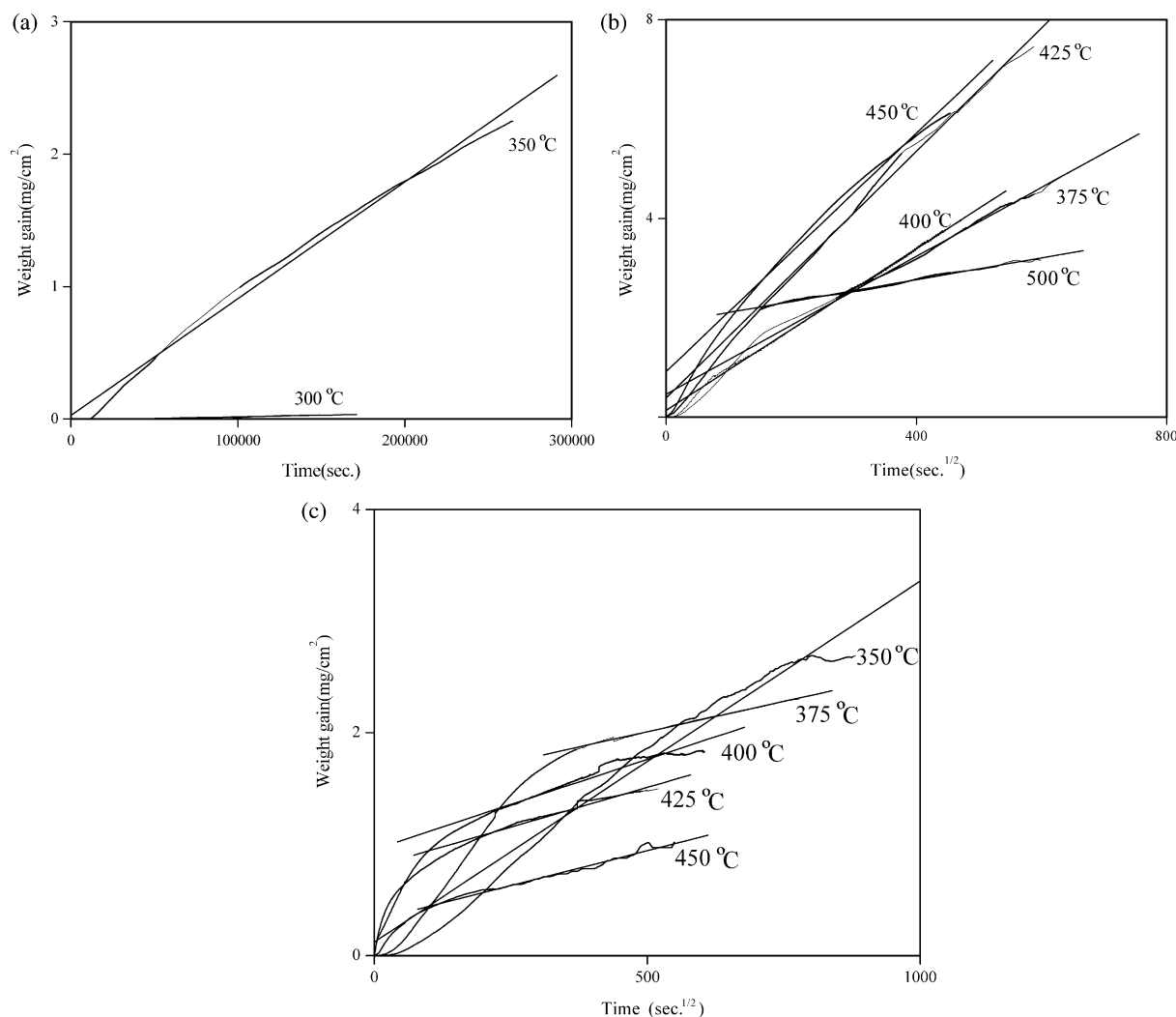


Fig. 2. Oxidation kinetics (weight gain as a function of time) measured from (a, b) Zr53 and (c) Zr65.

the three alloys studied, indicating this alloy has a high glass stability.

3.2. Oxidation kinetics

Thermogravimetric (TG) curves shown in parabolic plots for Zr53 and Zr65 over the temperature range of 300–500 °C are presented in Fig. 2(a)–(c). The oxidation of Zr53 exhibits a linear behavior at 300 and 350 °C, as shown in Fig. 2(a), suggesting that gas–metal interface reaction was the rate-determining step for Zr53 at $T \leq 350$ °C. Although not shown here, similar linear kinetics was also observed in Zr55 and Zr65 at 300 °C.

At higher temperatures, single-stage and two-stage parabolic rates were observed for the three BMGs, as shown in Fig. 2(b) and (c) for Zr53 at $T > 350$ °C and for Zr65 at $T \geq 350$ °C. The single-stage kinetics was fitted with a simple parabolic function, while the weight gain for two-stage kinetics started to increase sharply within few hours, and then followed by a steady-state stage. It is

obvious that solid-state diffusion was the rate-limiting step for all the BMGs at temperatures > 350 °C. The oxidation rate constants (K_p values) measured from the steady-state stage for all the alloys are tabulated in Table 1. The oxidation kinetics of BMGs is noted not to follow a simple Arrhenius equation; in fact, K_p values fluctuated with increasing temperature. This means that the oxidation of glassy alloys initially has a faster rate at the temperature

Table 1
Oxidation rate constant, K_p ($\text{g}^2/\text{cm}^4/\text{s}$) for the three Zr-BMGs

T, °C	Zr53	Zr55	Zr65
300	Linear	Linear	Linear
350	Linear	1.16×10^{-11}	1.05×10^{-11}
375	4.82×10^{-11}	2.06×10^{-11}	1.39×10^{-12}
400	6.61×10^{-11}	8.76×10^{-12}	2.62×10^{-12}
425	1.54×10^{-10}	3.65×10^{-12}	2.02×10^{-12}
450	1.44×10^{-10}	8.08×10^{-13}	1.59×10^{-12}
500	4.80×10^{-12}	4.21×10^{-13}	–

below T_g , but exhibited a slower rate once the temperature is above T_g . In fact, Köster et al. [9] conducted the oxidation of a Zr-base BMG and its nanocrystalline counterpart and found that the kinetics could be influenced by the difference of the free enthalpy; glassy alloy has a much higher enthalpy than the crystalline alloy, thereby leading to a faster oxidation rate in BMGs. At a higher oxidation temperature, a larger amount of nanocrystals is expected to be produced, thereby the lower the K_p values obtained through TGA tests.

3.3. Microstructure and phase constitution in oxide scales

X-ray diffraction pattern from the scale on Zr53 at 500 °C for 100 h shows the scale consisting of mainly t-ZrO₂ and m-ZrO₂, and minor amounts of NiO and Cu₂O (Fig. 3). The amount of t-ZrO₂ gradually reduced and m-ZrO₂ slightly increased from the oxidized surface to the interior of scale. It is of interest to note that the Zr53 substrate completely transforms into crystalline Zr₂Cu phase, indicating the occurrence of crystallization.

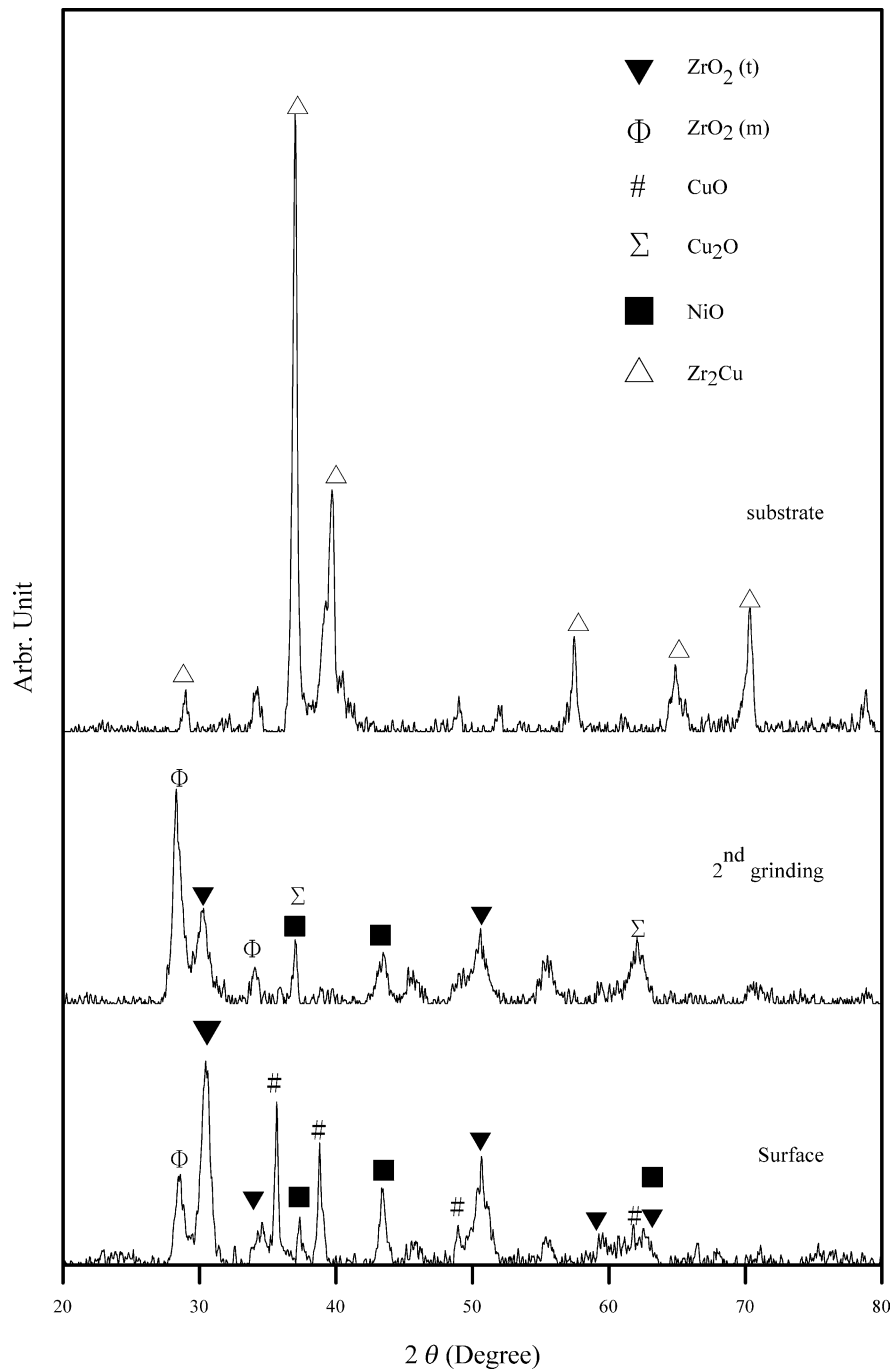


Fig. 3. XRD spectra from the scale formed on Zr53 at 500 °C for 100 h.

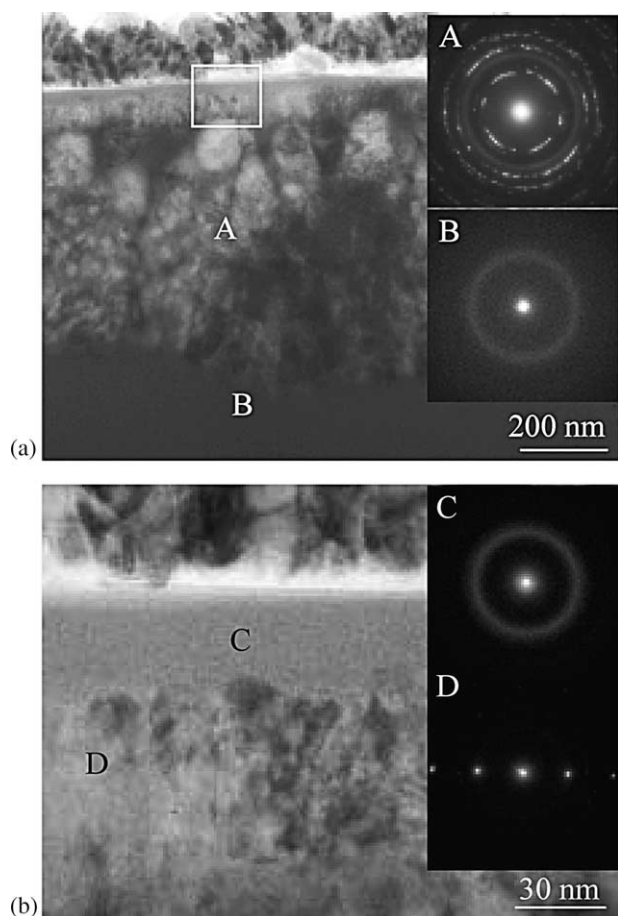


Fig. 4. (a) Cross-sectional TEM image for Zr53 oxidized at 300 °C for 73 h, and the corresponding selected-area diffraction patterns; (b) a high-magnification interface, and the corresponding selected-area diffraction patterns.

Additional analyses of the oxide scale formed on the Zr53 sample oxidized at 300 °C for 73 h were performed using TEM (with camera length = 80 cm); this result is presented in Fig. 4. A typical cross-sectional TEM image is given in Fig. 4(a), showing the oxide scale is over 500 nm thick. Selected-area diffraction (SAD) patterns from the oxide layer and matrix are shown in Fig. 4(b) and (c). Some crystalline structure (Area A) consisting of mainly copper oxide was detected in the scale while the substrate (Area B) maintained an amorphous structure. At a higher magnification (Fig. 4(b)), the oxide scales show a smooth, upper layer (~26 nm thick, Area C) and a nano-sized oxide-grain (Area D) lower layer. SAD patterns from different areas, also inserted in Fig. 4(b), reveal that the upper oxide layer is amorphous, but the lower layer contains a texture of partially crystalline t-ZrO₂.

XRD spectra from the surface scale formed on Zr65 oxidized at 375 °C for 168 h is shown in Fig. 5. Nickel oxide was absent in the scale, as similar to the result of Zr55 at 400 °C, but CuO did form in the exterior scale.

In addition, t-ZrO₂ was observed with a higher peak-intensity. However, the amount of t-ZrO₂ became weak after grinding into the interior scale, indicating that t-ZrO₂ gradually decreased with increasing grinding times. Unlike Zr55 which always has an amorphous substrate upon oxidation [12], Zr65 substrate transformed to Zr₂Cu and ZrAl crystalline phases even at an oxidation temperature below T_g (368 °C).

Surface scale formed on Zr65 is depicted in Fig. 6. Fine granular oxides are observed, and its grain size gradually increases with increasing temperature. To examine compositional difference for possible oxides formed on the alloys, some point-to-point EDX analyses were performed and the results are tabulated following the micrograph. According to the results, granules formed on Zr65 are copper-rich whereas other areas consist of approximately 23% zirconium and 66% oxygen. Thus, it is reasonable to assume that oxides formed on Zr-base BMGs were mostly zirconium and copper oxides.

BEI micrographs of the cross-sectional scales formed on both Zr55 and Zr65 at various temperatures are shown in Fig. 7. The images reveal a dark-layered scale of zirconium oxide and significant spallation of the oxide layer occurs in Zr55. It is also noted that the scale/substrate interface is non-planar, suggesting that inward diffusion of oxygen to the reaction front is the predominant rate-controlling step, similar to the previous result [12].

3.4. Short-term oxidation

To understand the initial oxidation, short-term oxidation tests were performed. Small and high-density granules (Fig. 8) are clearly observed on the surface of Zr53 oxidized at 425 °C for 2 h. XRD analyses show that both t- and m-ZrO₂ formed in the early stage of oxidation, and the peak-intensity of t-ZrO₂ was higher than that of m-ZrO₂. Also, Zr₂Cu was exclusively found in the substrate, indicating crystallization has occurred during the short-term test, even though the temperature is below T_x . The presence of oxygen apparently accelerates crystallization. By contrast, in the case of Zr55, oxide granules sparsely formed at 375 °C for 4 h (Fig. 9) and the corresponding XRD spectra shows only t-ZrO₂ on the surface. Thus, it is concluded that t-ZrO₂ is the first oxide phase formed during the initial stage of oxidation and the substrate remains amorphous for Zr55. In the case of Zr65 (Fig. 10), when the alloy oxidized at 425 °C for 2 h a similar result to Zr53 was observed; however, crystalline ZrAl was also present in the substrate.

3.5. Phase transformation study

According to the Zr–O phase diagram [13], there exists a single ZrO_{2-x} oxide in which the concentration of oxygen varies with temperature. The black nonstoichiometric zirconium oxide, which is oxygen deficient [Vö],

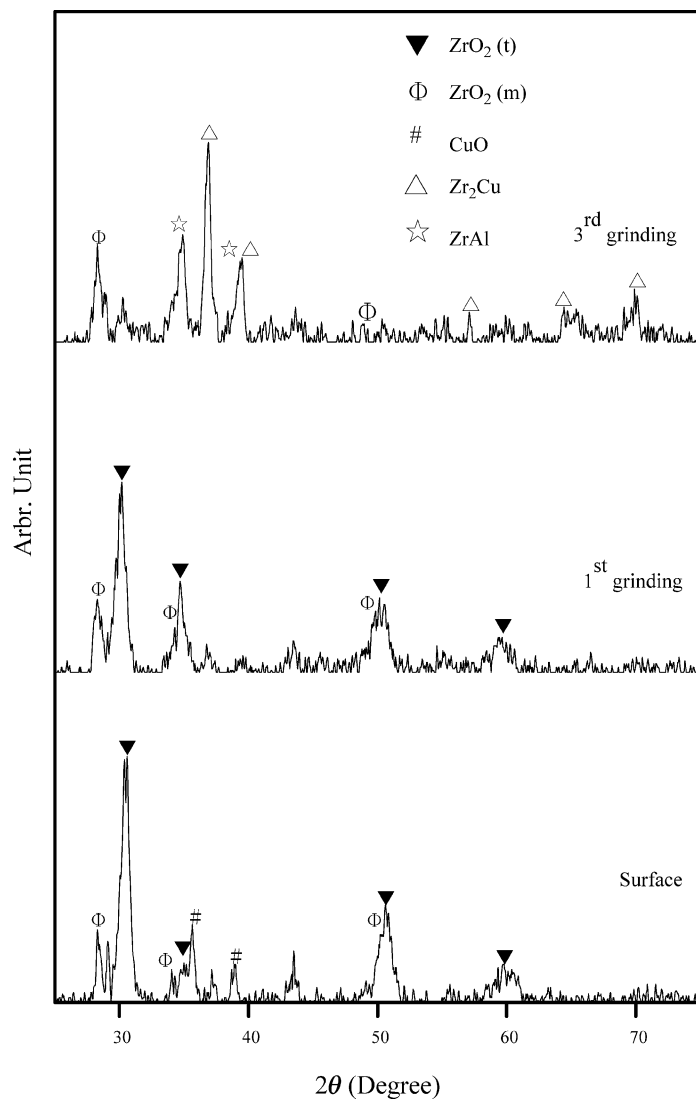
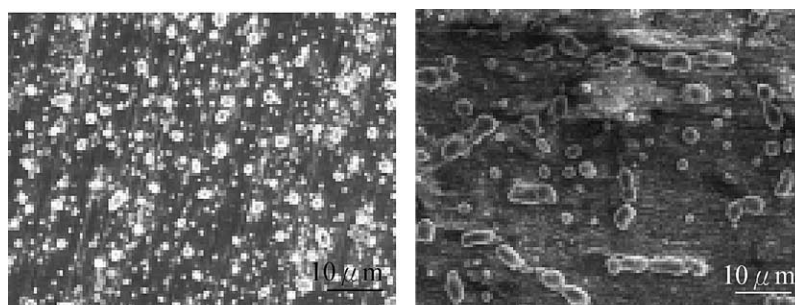


Fig. 5. XRD spectra of the scales formed on Zr65 at 375 °C for 168 h.



(a)

(b)

at. %	Zr	Cu	Al	Ni	O
A	15.81	15.80	3.02	2.25	63.11
B	23.32	2.90	4.59	2.85	66.33

Fig. 6. SEM of the scale on Zr65 oxidized in air at (a) 300 °C for 480 h, and (b) 375 °C for 168 h, and the corresponding EDX analyses.

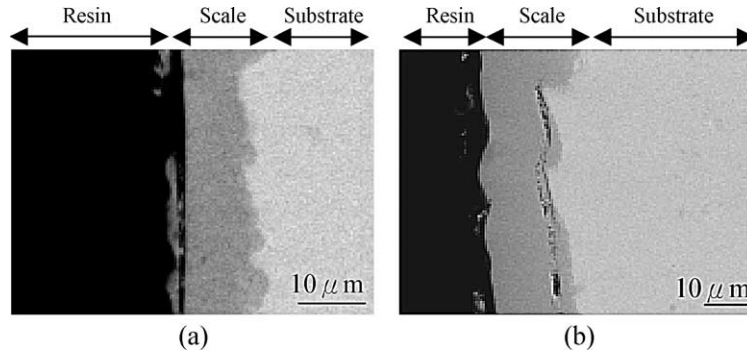


Fig. 7. Cross-sectional BEI micrographs of (a) Zr55 oxidized 60 h at 400 °C, and (b) Zr65 oxidized 168 h at 375 °C.

belongs to N-type semiconductor [11,12]. It is also known that there are three well-defined polymorphs of pure ZrO_2 with monoclinic, tetragonal, and cubic structures [5,13,14]. The monoclinic ZrO_2 is stable at temperatures below 1000–1200 °C, the tetragonal ZrO_2 is stabilized at higher temperatures, and cubic ZrO_2 is stable only at $T > 1500$ °C. Since t- ZrO_2 stabilized at high temperatures, its presence in BMGs and crystalline can be considered as a metastable phase, probably stabilized by another transition element [7]. In contrast, m- ZrO_2 is thermodynamically stable. To understand the role of

t- and m- ZrO_2 during oxidation, it is of great interest to compare the formation tendency of both oxides. Using JCPDS files and neglecting the possible preferred orientation of the scales, XRD-diffraction peak heights for the strongest intensity of t- ZrO_2 and m- ZrO_2 at $2\theta = 30.2$ and 28.10° , respectively, were chosen and the calculated results are summarized in Table 2. As shown in Table 2, the ratio of A (m) in Zr65 is higher than that in other alloys, suggesting that the preferential formation of m- ZrO_2 on a Zr-enriched substrate. It is also noted that the amount of m- ZrO_2 in oxide scale on a sample

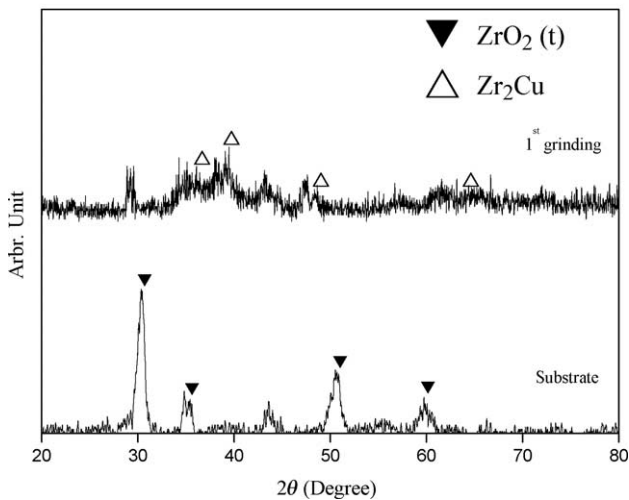
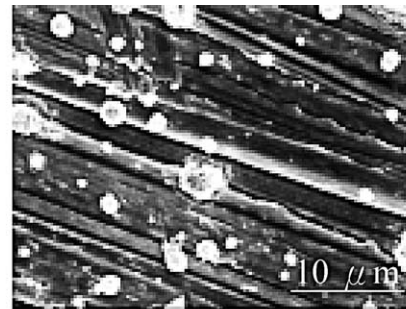
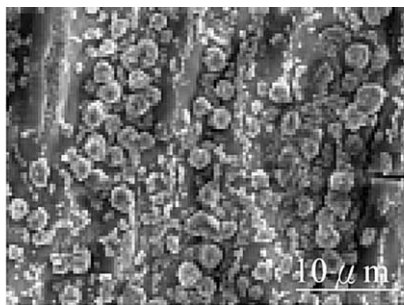


Fig. 8. Oxide scale formed on Zr53 at 425 °C for 2 h, and its corresponding XRD spectra.

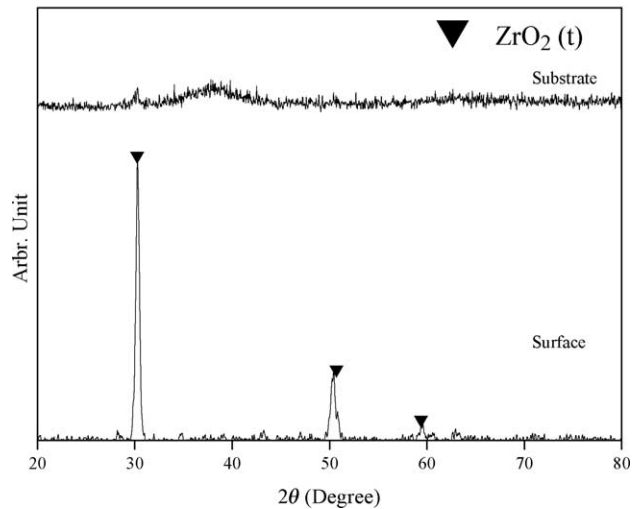


Fig. 9. The surface scale formed on Zr55 at 375 °C for 4 h, and its corresponding XRD spectra.

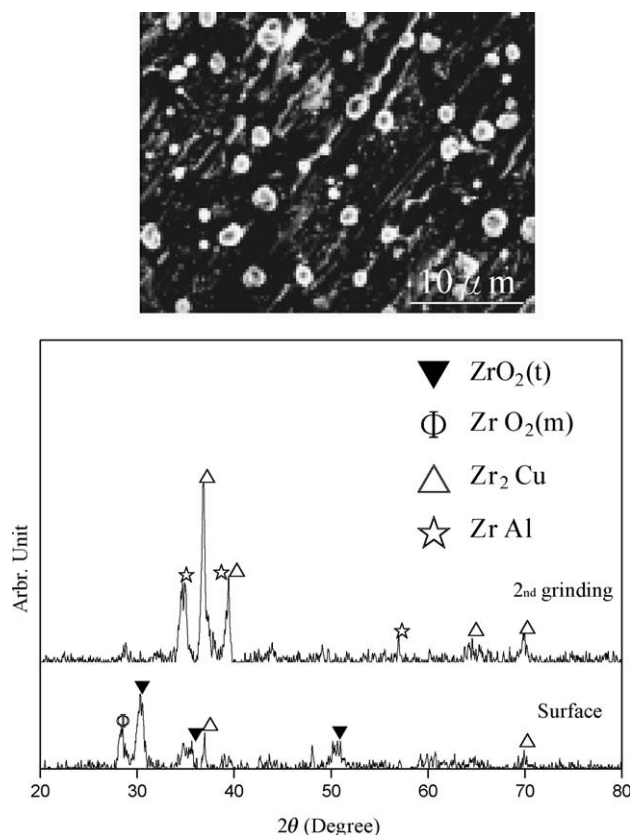


Fig. 10. The surface scale formed on Zr65 at 425 °C for 2 h, and its corresponding XRD spectra.

oxidized for long time is significantly greater than that in oxidized for short time, indicating that m-ZrO₂ was thermodynamic stable with exposure time. This observation is consistent with that reported by Asami et al. [5].

Table 2

Ratios of XRD peak for tetragonal and monoclinic zirconium oxides formed on BMGs after oxidation

Long-term	Zr53 (425 °C, 96 h)	Zr55 (425 °C, 96 h)	Zr65 (425 °C, 96 h)
A(t)	81.76	45.59	34.40
A(m)	26.15	7.31	15.64
$\frac{A(m)}{A(t) + A(m)}$	0.242	0.138	0.313
Short-term	Zr53 (425 °C, 2 h)	Zr55 (375 °C, 4 h)	Zr65 (425 °C, 2 h)
A(t)	58.28	92.23	32.18
A(m)	0	0	15.97
$\frac{A(m)}{A(t) + A(m)}$	0	0	0.332

A(t) and A(m) are calculated from areas and peak heights for t- and m-ZrO₂ phases at $2\theta = 30.2$ and 28.1° , respectively.

4. Conclusion

The oxidation behavior of three Zr-based bulk metallic glasses, Zr53, Zr55, and Zr65, over the temperature range of 300–500 °C in air was characterized. Several conclusions were summarized as follows:

1. Oxidation kinetics of the BMGs followed a linear behavior at 300 °C, but could be fitted by a parabolic law above at $T > 350$ °C. Zr53 still followed a linear behavior at 350 °C.
2. T- and m-ZrO₂ were commonly observed as the oxidizing products. Oxide scale formed on high Zr-containing BMG alloys always consisted of significant amount of m-ZrO₂.
3. Nanograins were observed immediately beneath the amorphous oxide scale in Zr53 after oxidation, indicating that phase transformation took place even at a very low temperature.

Acknowledgements

Financial support by the National Science Council of Republic of China (the Grant No. NSC91-2216-E-019-002) is gratefully acknowledged. The work performed by TGN was under the auspices of the US Department of Energy by the University of California, Lawrence Livermore National Laboratory under Contract No. W-7405-Eng-48. Special thanks to Department of Engineering and System Science, National Tsing-Hua University for the transmission electron microscope work.

References

- [1] Inoue A. Mater Sci Forum 1995;691:179–81.
- [2] Inoue A. Acta Mater 2000;48:279–306.
- [3] Inoue A. Bulk amorphous alloys—practical characteristics and applications. Materials science foundations series, vol. 6. Zurich, Switzerland: Trans Tech.; 1999.
- [4] Dhawan A, Raetzke K, Faupel F, Sharma SK. Bull Mater Sci 2001; 24(3):281–3.
- [5] Asami K, Kimura HM, Hashimoto K, Masumoto T. Mater Trans JIM 1995;36(7):988–94.
- [6] Sharma SK, Strunskus T, Ladebusch H, Faupel F. Mater Sci Eng A 2001;304–306:747–52.
- [7] Aoki K, Masunoto T, Suryanarayana C. J Mater Sci 1986;21:793–8.
- [8] Schneider S, Sun X, Nicolet M-A, Johnson WL. In: Otonari MA, editor. Science and technology of rapid solidification and processing. Netherlands: Kluwer Academy Publishers; 1995. p. 317–26.
- [9] Köster U, Zander D, Triwikantoro, Rüdiger A, Jastrow L. Scripta Mater 2001;44:1649–54.
- [10] Fan C, Li C, Inoue A. J Non-Cryst Solids 2002;312–314:617–21.
- [11] Inoue A, Zhang T, Masumoto T. Mater Trans JIM 1990;31:177.
- [12] Kai W, Hsieh HH, Nieh TG, Kawamura Y. Intermetallics 2002;10: 1265–70.
- [13] Kofstad P. High temperature corrosion. London: Elsevier; 1988.
- [14] Douglass DL. The metallurgy of zirconium, Internet. Vienna: Atomic Energy Agency; 1971.